Petroleum Science 21 (2024) 609–620

Contents lists available at ScienceDirect

Petroleum Science

journal homepage: www.keaipublishing.com/en/journals/petroleum-science

Original Paper

Study on the clogging mechanism of punching screen in sand control by the punching structure parameters

Fu-Cheng Deng [a, *], Fu-Lin Gui [a], Bai-Tao Fan [b], Lei Wen [a], Sheng-Hong Chen [c], Ning Gong [d], Yun-Chen Xiao [a], Zhi-Hui Xu [a]

[a] Yangtze University, Jingzhou, 434023, Hubei, China
[b] CNOOC Research Institute Ltd., Beijing, 100028, China
[c] CNOOC Ener Tech-Drilling & Production Co., Tianjin, 300457, China
[d] Tianjin Branch of CNOOC Ltd., Tianjin, 300459, China

ARTICLE INFO

Article history:
Received 20 March 2023
Received in revised form
26 April 2023
Accepted 16 August 2023
Available online 25 August 2023

Edited by Jia-Jia Fei

Keywords:
Punching screen
Plugging
CFD-DEM
Size parameter
Sand control

ABSTRACT

As an independent sand control unit or a common protective shell of a high-quality screen, the punching screen is the outermost sand retaining unit of the sand control pipe which is used in geothermal well or oil and gas well. However, most screens only consider the influence of the internal sand retaining medium parameters in the sand control performance design while ignoring the influence of the plugging of the punching screen on the overall sand retaining performance of the screen. To explore the clogging mechanism of the punching screen, this paper established the clogging mechanism calculation model of a single punching screen sand control unit by using the computational fluid mechanics-discrete element method (CFD-DEM) combined method. According to the combined motion of particles and fluids, the influence of the internal flow state on particle motion and accumulation was analyzed. The results showed that (1) the clogging process of the punching sand control unit is divided into three stages: initial clogging, aggravation of clogging and stability of clogging. In the initial stage of blockage, coarse particles form a loose bridge structure, and blockage often occurs preferentially at the streamline gathering place below chamfering inside the sand control unit. In the stage of blockage intensification, the particle mass develops into a relatively complete sand bridge, which develops from both ends of the opening to the center of the opening. In the stable plugging stage, the sand deposits show a “fan shape” and form a “V-shaped” gully inside the punching slot element. (2) Under a certain reservoir particle-size distribution, The slit length and opening height have a large influence on the permeability and blockage rate, while the slit width size has little influence on the permeability and blockage rate. The microscopic clogging mechanism and its law of the punching screen prevention unit are proposed in this study, which has some field guidance significance for the design of punching screen and sand prevention selection.

1. Introduction

Most oil fields in our country contain loose sandstone reservoirs, which are widely distributed in the country, and their development potential is large. Loose sand reservoirs are weakly consolidated or unconsolidated and have high permeability, high sand production in the process of production possibilities, and sand for the integrity of the development in the borehole, that may cause harm to personnel and equipment safety (Lu et al., 2022; Yao et al., 2021) increasing development costs and difficulties (Deng et al., 2017). At present, most in need of sand control wells adopt a mechanical screen pipe for sand control. A mechanical screen as a simple and effective means of sand control, often used in oil and gas field or geothermal well development, is also an important means to increase production capacity. A punched screen, as in most cases, is a widely used high-quality screen (Li, 2019) compared to a slotted screen. The characteristic of the punching screen is to increase the seepage area of the screen (Deng et al., 2021), which indirectly improves the well fluid flow rate. However, most screens only consider the influence of the sand retaining medium inside the

* Corresponding author.
E-mail address: dengfucheng128@163.com (F.-C. Deng).

https://doi.org/10.1016/j.petsci.2023.08.017

screen when considering its sand control performance and ignore the sand retaining effect of the punching screen as a sand retaining element directly in contact with the formation (Yin et al., 2021). At present, there have been few studies on the mechanisms and influencing factors of punching screen plugging. In the actual production process, due to the plugging of the punching screen, the permeability decreases, which leads to a significant decline in the production capacity (Deng et al., 2019, 2022). Fig. 1 shows a schematic diagram of punching screen tube blockage.

Most current research on sand control wellbore clogging has been focused on sand control media inside the sand control screen for sand-blocking experiments (Li and Wu, 2022; Li et al., 2022). Deng et al. (2017a, b) simulated the clogging process and clogging mechanisms of the metal mesh screen in the process of microparticle sand control using an oil and gas well sand control simulation experimental device and determined the influence of the microparticle composition and sand discharge sequence on the clogging mechanisms of the metal mesh screen. Dong et al. (2016) conducted experiments on the blockage mechanisms and laws of the gravel layer, focusing on the quantitative change laws of different production conditions, and formed a quantitative prediction method for the degree of blockage. Yang (2018) developed an experimental device for evaluating the blockage characteristics of loose sand and mudstone interbedded sand control screens and realized the stepwise establishment of displacement pressure differences. Through a comparative analysis of wellbore pressure, production and permeability in the process of formation sand production, simulation experiments and evaluations were conducted on the blockage characteristics and mechanisms of sand control wellbores.

These studies have simulated the process of screen plugging by means of experiments (Deng et al., 2018). However, from the perspective of experiments, we can only analyze the screen permeability, sand production rate and other data from a macro perspective and cannot observe the screen-blocking process and the screening process from a microscopic perspective (Zhang et al., 2022). With the continuous development of computer technology, CFD-DEM technology has been widely used in various fluid-solid kinematics simulations (Qing et al., 2019; Cheng et al., 2018; Wang et al., 2022). Song et al. (2021) simulated the microscopic formation principle of sand bridging under hydrodynamics. The influence of the friction coefficient between the sand particles and the screen on the stability of the sand bridge on the slotted screen was investigated. Therefore, from a microscopic perspective, this paper uses the computational fluid dynamics-discrete element (CFD-DEM) combined method to study the clogging mechanisms of the punching unit from the perspective of punching processing control to provide guidance for the dimension control of punch screen machining.

2. CFD-DEM combined method

The CFD-DEM method does not require a complex constitutive relationship between the stress and strain tensors of discrete particles under different flow conditions; therefore, it is widely applicable to various flow systems. In addition, the generated microscopic information, such as the force on a single particle and its motion trajectory, is helpful to understand the mechanisms of particle fluid flow.

With the continuous progress of computer technology, the combined between computational fluid dynamics (CFD) and the discrete element method (DEM) has been introduced into various fluid-solid kinematic simulations. The CFD-DEM combined uses the discrete element method and Hertz contact theory to calculate the particle motion morphology and uses Newton's motion theorem to analyze the particle motion process in the sieve tube (Feng et al., 2021). The DEM simulation of particle flow is based on individual particles, while the CFD simulation of fluid is based on computational units. According to Xu and Yu (1997), at each time step, Fluent solves the relevant parameters of the continuous flow field, passes the data to the EDEM solver, calculates the forces between the particle phases, couples the calculation with the particle equations of motion, and obtains the discrete phase particle. The Fluent solver obtains the data from the EDEM solver and solves the flow field with particle phases, updates the flow region, and cycles the operation to the next time step (Li et al., 2020), as shown in Fig. 2.

2.1. Control equations of particle flow

The solid phase is considered a discrete phase and is described by the DEM method originally proposed by Cundall and Starck. In the DEM method, the particles have two types of motion: translation and rotation, both of which follow Newton's second law of motion. During its motion, the particle may collide with its neighbors or the wall of the tube and interact with the surrounding fluid, through which it exchanges momentum. At any time t, the equations controlling the translational and rotational motion of particle i in this flow system are (Kuang et al., 2020):

$$m_i\frac{\mathrm{d}v_i}{\mathrm{d}t}=f_{p-f,i}+\sum_{j=1}^{k_i+k_\omega}\left(f_{\mathrm{c},ij}+f_{\mathrm{d},ij}\right)+m_ig \tag{1}$$

$$I_i\frac{\mathrm{d}w_i}{\mathrm{d}t}=\sum_{j=1}^{k_i+k_\omega}\left(T_{t,ij}+T_{\mathbf{r},ij}\right)+T_{ls,i} \tag{2}$$

where, m_i, I_i, v_i and ω_i are the mass, moment of inertia, translational

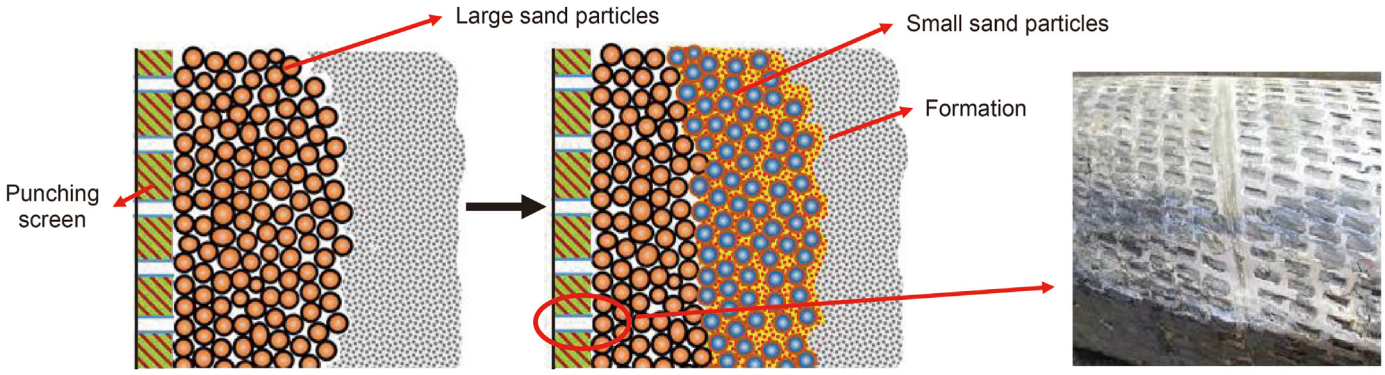

Fig. 1. Schematic diagram of punching screen blockage.

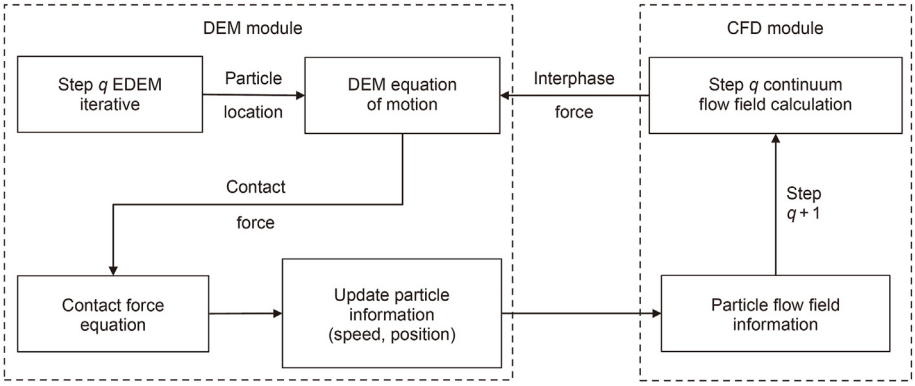

Fig. 2. CFD-DEM combined flowchart.

velocity and angular velocity of particle i, respectively. $f_{p-f,i}$ denotes the particle fluid force. $f_{c,ij}$ and $f_{d,ij}$ are the elastic and viscous contact damping forces between particle i and particle or wall j, respectively. $m_i g$ is the force of gravity (T_{ij} is the torque exerted on particle i due to particle or wall j).

2.2. Fluid governing equation

The model treats the fluid as a continuous phase and is solved by the N–S equation. The mass conservation equation and momentum conservation equation are shown in Eqs. (3) and (4).

$$\frac{\partial}{\partial t}\left(\alpha_f \rho_f\right) + \nabla \cdot \left(\alpha_f \rho_f v_f\right) = 0 \tag{3}$$

$$\frac{\partial}{\partial t}\left(\alpha_f \rho_f v_f\right) + \nabla \cdot \left(\alpha_f \rho_f v_f v_f\right) = -\alpha_f \nabla p - \alpha_f \mu_f \nabla^2 v_f + F^p \tag{4}$$

where α_f is the volume fraction of fluid, dimensionless. ρ_f, v_f, p and μ_f are fluid density, fluid velocity, fluid pressure and fluid viscosity, respectively. F^p is the original momentum term, that is, the physical force of each fluid element or the force of sand particles in the fluid element on the fluid, N/m^3.

2.3. Fluid–sand interaction force

The interaction force between the fluid and sand includes the drag force, lift force, buoyancy force, gravity force, pressure gradient force, Basset force, etc. (Ismail et al., 2020). In the screen blockage model, the drag force is the main force of sand movement guided by the fluid, which is also the focus of this paper. The drag force is mainly expressed in the interaction between fluid and sand, which is often calculated by empirical models, among which the Di Felice model is the most common model to study the particle-blocking problem. Its expression is shown in Eq. (5):

$$\begin{cases} F_{p,f} = \frac{1}{2}\pi C_d \rho_f r_p^2 \left|u_p - u_f\right| \varepsilon_f^{(2-\chi)} \\ \chi = 3.7 - 0.65 \exp\left[-\frac{(1.5 - \lg Re_p)^2}{2}\right] \end{cases} \tag{5}$$

where ρ_f is the fluid density, kg/m^3; u_f is the fluid velocity, m/s; Re_p represents the Reynolds number of fluid grit; r_p represents the sand radius, m; u_p represents the sand velocity, m/s; C_d represents the drag coefficient, dimensionless; $C_d = \left(0.63 + \frac{4.8}{\sqrt{Re_p}}\right)^2$; χ represents the correction factor; and ε_f is the porosity.

3. Clogging mechanism of the sluicing unit

3.1. Model of punching and seam element

Due to the special filtration structure of the punching seam screen, it increases the opening area of the conventional slit and wire winding (Zhang, 2017) and has high external extrusion strength. It is in direct contact with the formation fluid, which plays an important role in the production. Combined with the production site data, there is no unified standard for the production parameters, such as seam length, seam width and opening width. The sizes that manufacturers can process are seam lengths of 8, 9, 10, 11 and 18 mm; seam widths of 3–5 mm; and opening heights of 0.2, 0.3, 0.4, 0.5 mm. In this paper, the punching unit model was established at 1:1 according to the upper punching unit of the punching screen, as shown in the local enlarged view of the punching screen in Fig. 3(a), and its 3D model is shown in Fig. 3(b). The blue arrows show the entry, while the red arrows indicate the exit. The x, y, and z axes all have a common zero point and are orthogonal to one another. The dimensions of each part were 11 mm in seam length, 4 mm in seam width and 0.3 mm in opening height.

3.2. Simulation parameter settings

In combination with relevant literature (Li et al., 2021) and field data, this paper obtained the following parameters: The discrete phase parameter is based on the distribution of sand grain size in the formation at a certain well depth in the Shahejie reservoir; the median particle size of discrete phase parameters is 252 μm, and the heterogeneity coefficient UC = 1.5. The particle-size distribution is shown in Fig. 4. The morphology of the particles will be designed in the study to more realistically represent stratigraphic sand, and this test employs sand particles with a commonly used sphericity of 0.8. Poisson's ratio is 0.3, density is 2650 kg/m^3, elastic modulus is 100 MPa, coefficient of restoration is 0.3, and friction coefficient is 0.5. The fluid phase is water, and its density is 998.2 kg/m^3. Considering the element body swirl and eddy current generation, in the calculation of the k-ε turbulence model, the inlet condition is a velocity inlet and the study is based on a field flow velocity of 1.2 m/s the outlet condition is the pressure outlet, and the inlet outlet turbulence intensity control is 5%.

3.3. Model verification

In order to verify the CFD-DEM simulation model, this

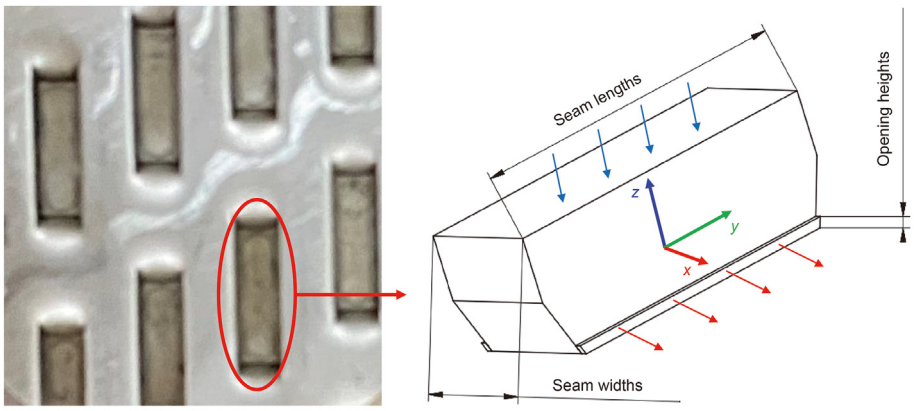

(a) Local enlarged view of the punching casing **(b)** 3D model of punching slot element

Fig. 3. Establishment of the model of punching and seam element.

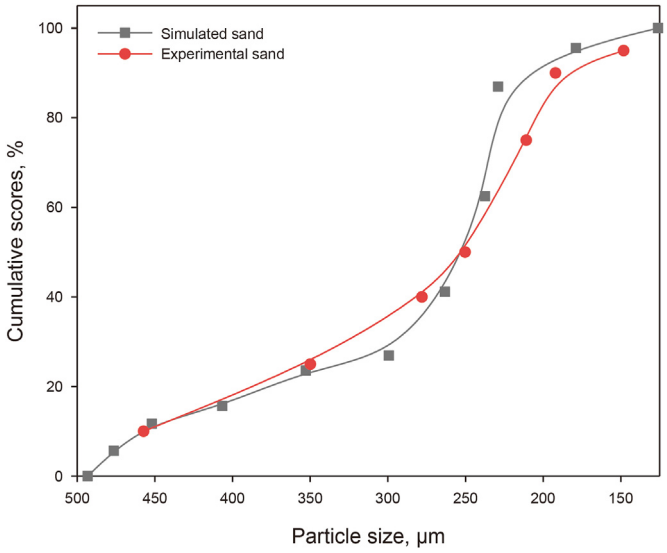

Fig. 4. Simulated and experimental sand particle-size distribution.

experiment uses a punching unit with an opening height of 0.3 mm that is more analyzed in the simulation to carry out research. And only a single slit is left in the punching sheet to block the remaining seams to ensure that the parameters of the experiment and the simulation are consistent. The screen segment is shown in Fig. 5.

Fig. 6 shows the sand clogging state of the punching sand retaining unit at different times in the experiment and simulation. It can be seen from Fig. 6, the sand particles have the same accumulation state on the sand retaining unit of the punching screen. They all develop from the 'sand arch' accumulation at both ends of the opening to the inside of the sand retaining unit, showing a symmetrical distribution until the whole sand retaining unit of the punching screen is filled. However, the time periods of simulation and experiment are different. The main reasons are as follows: ① The size of simulation model and experimental sample is different; ② It caused by the pipeline length and flow in the experiment.

Fig. 7 shows the comparison of pressure difference and flow rate between experiment and simulation. It can be seen from Fig. 7(a)–(b) that there is a certain relationship between the pressure difference and the flow rate between the simulation and the experiment, and the overall change trend is similar. The process can be roughly divided into three stages: pressure rising and initial blockage; a sharp increase in pressure and increased blockage; pressure changes tend to be stable and block stability. The final pressure difference of the experiment is 1.33 MPa, and the final pressure difference of the simulation is 1.19 MPa. In the experiment, the flow rate is 0.57 L/min when the blockage is balanced, and the flow rate is 0.65 L/min when the blockage is balanced in the simulation. The difference between the pressure difference and the flow rate is small and within the acceptable range.

Fig. 8 is the comparison of permeability change with time. It can be seen from the figure that the permeability in the simulation and experiment is similar. Although there are some differences in the early permeability changes due to the uncontrollable factors of the experiment, the final permeability is relatively similar, the difference is less than 10%, and the error is within the acceptable range. In summary, it is reliable to use the model for coupling simulation to predict the clogging process and permeability of the punching screen.

3.4. Research on the blocking process

At present, most research is mainly based on macroscopic sand retaining experiments in a sand retaining medium, and there is still a lack of systematic understanding of the microscopic sand retaining process and law of the sand retaining medium under the condition of flowing with fine silt. The clogging process of the punching slot unit generally presents three stages: $0-t_0$ beginning to clog, t_0-t_1 clogging aggravation, and t_1-t_2 clogging stabilities, as shown in Fig. 9. The permeability ratio presented in this paper refers to the ratio of the real-time permeability to the initial permeability of the fracture unit, which is dimensionless. The smaller the permeability ratio is, the higher the plugging degree of the unit.

Fig. 10 shows the distribution of particles at different time points calculated by the combined model, and the clogging process of the punching unit is shown in the figure. At the initial stage of blockage, the large particles move to the seam in the first place. However, at this time, the internal space is large, the large particles are subjected to the fluid force and impact the wall and seam, the large particles are bounced back into the slot unit, the fluid flushes the large particles to the seam, and so on. As the sand increases and the flow space decreases, as shown in the black dashed box in Fig. 11(b), the particles preferentially gather at the streamline gathering point below the chamfer of the punching slot element. As shown by the arrow in Fig. 11(a), the blockage develops from both ends of the seam to the center. Large particles (red particles) preferentially jam

Fig. 5. Using screen segment in experiment.

the seam, resulting in a decrease in permeability, resulting in an increase in the pressure difference between the entrance and exit of the punching unit, as shown in Fig. 11(a). At this time, the formation of a relatively loose and certain circulation bridge structure also plays a certain sand control role. Particles smaller than the size of the seam can pass through the seam, and the amount of sand is higher.

With the deepening of the degree of congestion, sand in the slot unit internally accumulates to a certain number, and the flow space is reduced. At the seam, the particle size of the larger particles forms a relatively complete sand bridge. In addition to the coarse particle size, sand cannot pass, some small particles also fail, and some small particles and smaller particles adhere to the larger particles formed near the particles. Then, the particles are combined and aggregate into larger particles, resulting in blockage, as shown in Fig. 10(b). At the same time, the pore-throat size between sand particles is gradually reduced so that the punching unit can block finer sand, the flow performance of particles becomes worse, the sand retaining performance is improved, the pressure difference inside and outside the punching unit increases sharply, the flow resistance increases, and the permeability decreases sharply.

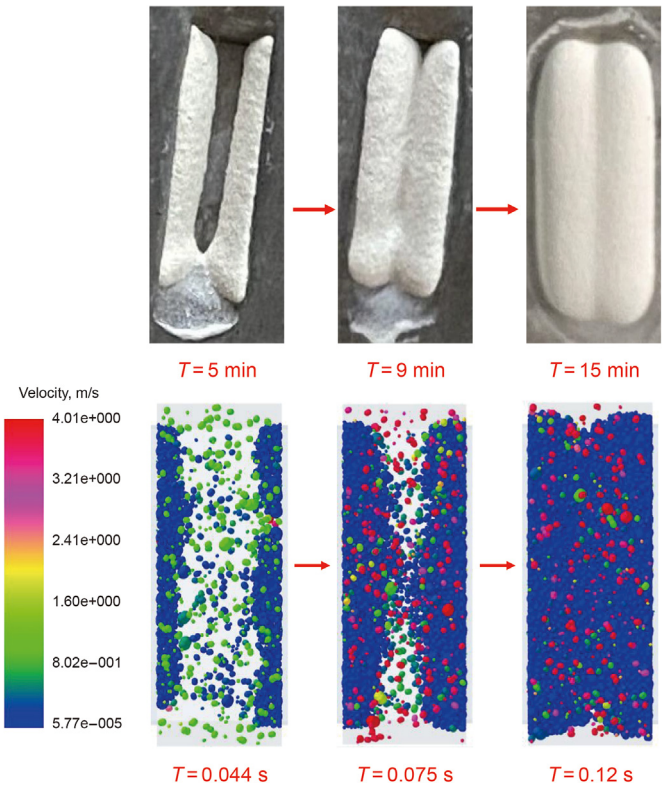

Fig. 6. Sand clogging state of punching unit.

The side sectional view in Fig. 12 corresponds to the *Y*-axis view in Fig. 3, and the top view corresponds to the *Z*-axis view in Fig. 3. The sand particles pile up in a “fan shape” behind the seam bridge, as shown in Fig. 12(a), and develop from the openings on both sides to the interior of the punching screen. As shown by the arrow in Fig. 12(b), with an increasing number of blocked particles, the particles at both ends continue to accumulate and gradually develop into a complete sand bridge. In the stable stage of blockage, as shown in Fig. 12(c), the “fan-shaped” stacking range behind the bridge increases, forming a stable bridge structure at the opening, and smaller particles move to the opening to reduce the diameter of the flow hole throat. From the top view in Fig. 12(d), the sand accumulation presents an “arch” accumulation, covering from both sides to the center, until it completely fills the punching screen, as shown by the arrow in Fig. 12(d). Fig. 11(e) shows that the “V" gully is formed in the middle of the punching screen. As mentioned in the above section, the chamfer structure in the punching screen makes the particles accumulate preferentially at the streamline gathering place below the chamfer, which also makes the accumulation speed of the particles at the streamline gathering place the fastest, making the particles finally present the blocking form, as shown in Fig. 12(f). Because the punched slot cell block sand structure space is limited, when this space filled with the invasion of sand piled up after blocking becomes increasingly serious, only a tiny part of the fine powder particles flows through the seam, causing a blocking balance and further reducing the pore-throat diameter. The sewing unit can stop more small particles, punching the slot at this time and the unit block sand ability is basically stable. Permeability stability is at a low level.

3.5. Two sand-blocking forms of punching screen unit

The opening height is selected according to the principle of Coberly (Gillespie et al., 2000). After analysis, when the opening height is selected properly, the blocking mechanism of the sand

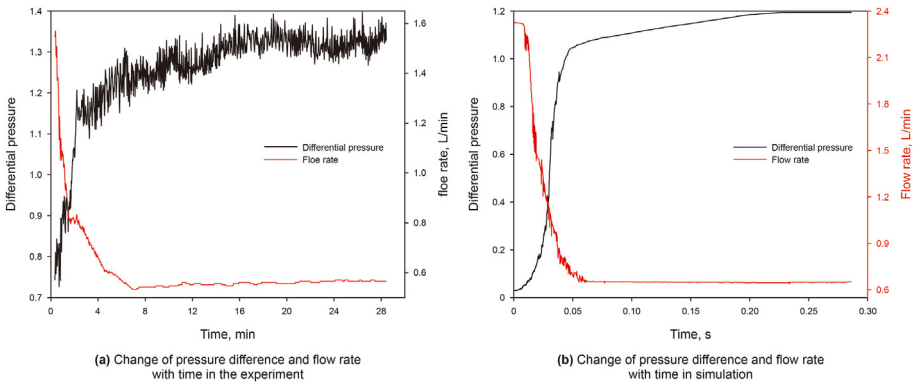

Fig. 7. Comparison of pressure difference and flow rate between experiment and simulation.

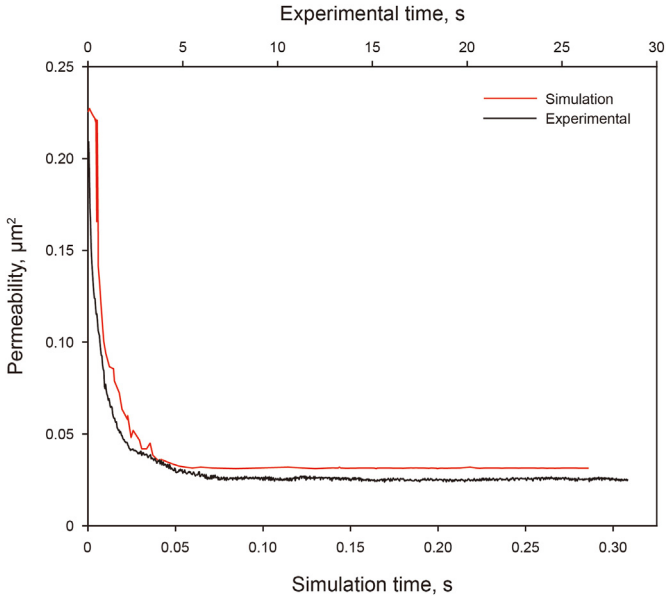

Fig. 8. Comparison of permeability change with time.

control unit of the punching screen can be divided into the following two sand-blocking forms:

(1) Large particles are stuck by the seam mouth-blocking sand: large diameter sand particles are stuck in the opening, the overflow area is reduced, and the particles gather here, forming a particle cluster caused by the blockage but also preventing other small diameter sand particles through the seam mouth, completely reducing the overflow area of the screen seam. As shown by the red circle in Fig. 13, the interaction between the particles point to the large particles stuck in the seam mouth.

(2) Sand grains bridge successfully: the blockage is formed after bridging at the opening of the punching unit due to the interaction between sand grains, but some of the small diameter sand grains at the seam opening can pass, as shown by the red circle in Fig. 14, and two grains form a bridging structure at the opening, causing blockage, and the force chain structure is shown in Fig. 14 (right).

4. Influence of different structure sizes on the blocking mechanism

4.1. Influence of different structural parameters on the blocking mechanism

With the wider application of punched screens, in the sand control process of oil and gas wells, the selection of structural parameters of punched screens is mostly determined by subjective experience, which is blind and random. In this case, under different formation conditions, there may be a relatively large gap in its sand control effect. This paper mainly focuses on the controllable parameters in processing as the analysis object, groups the punching units according to different size parameters, and obtains the results under different structural parameters.

4.1.1. Punching screen unit seam length dimensions

Considering only the influence of the seam length factor on the

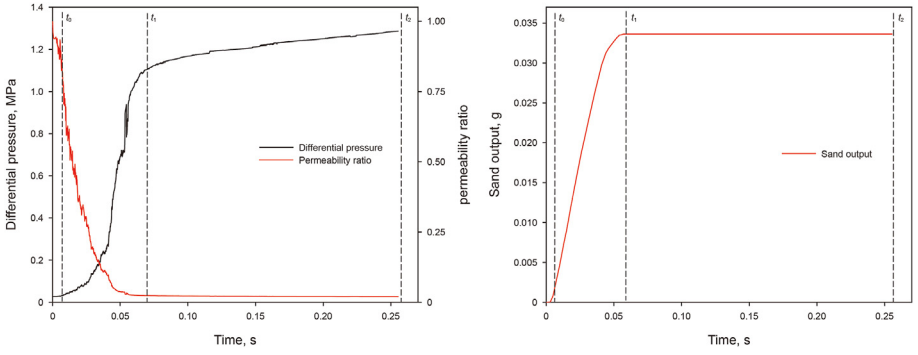

Fig. 9. Variation of pressure difference and permeability ratio and sand production during simulation.

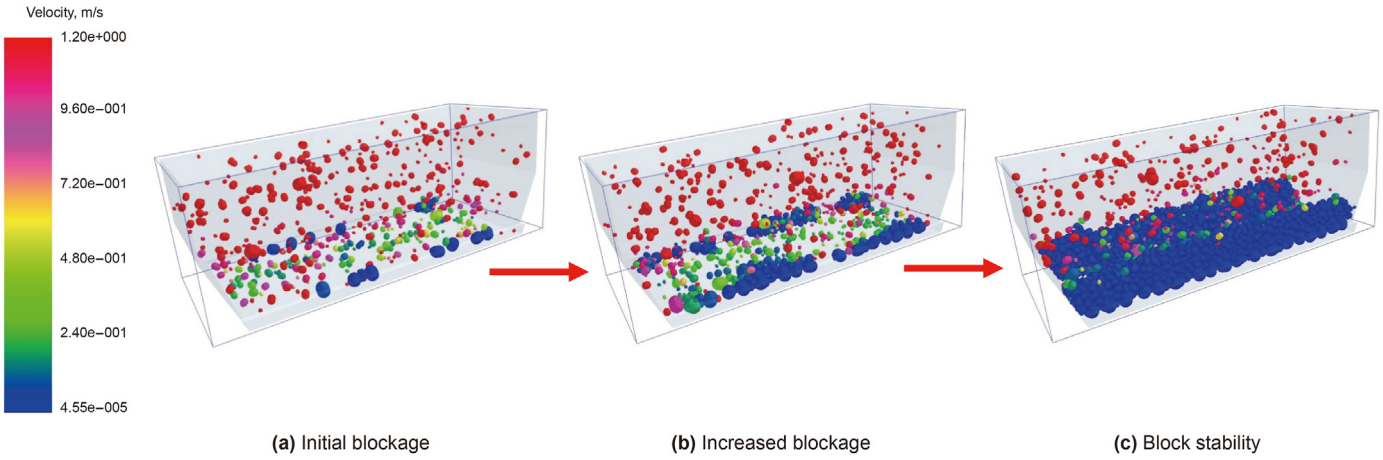

Fig. 10. Numerical simulation of the clogging process of sluicing elements.

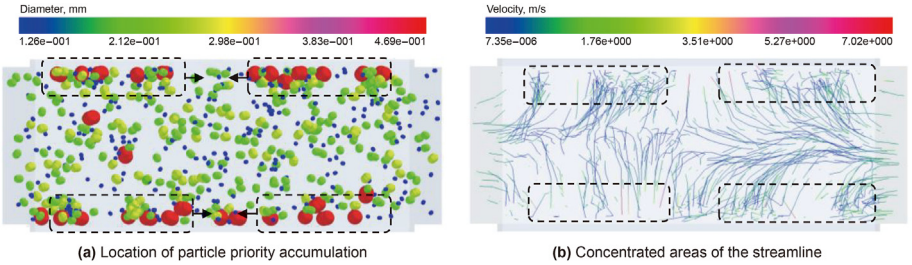

Fig. 11. Particle accumulation and velocity trajectory.

sand control performance of the punching slit unit, the control variable method is used at a slit width of 4 mm and an opening height of 0.3 mm, and commonly used slit length sizes, 8, 11, 15 and 18 mm, are used to start the study. In this case, the pressure difference and penetration rate ratio are shown in Fig. 15(a), in which the penetration rate ratio of the punching slit unit decreases rapidly and is low, then decreases slowly and finally stabilizes. With the increase in seam length, the rate of penetration rate ratio reduction decreases, and the difference between penetration rate ratio at the time of reaching stability is not significant, and all remain in a low range: 0.023, 0.020, 0.031, and 0.024, respectively. This shows that the clogging of the punching unit mainly occurs in the early stage, and with the continuation of production, although the clogging is gradually aggravated, the change in the clogging degree slows down. There is a significant difference in the pressure difference in the simulation process. With increasing seam length, the increasing rate of the pressure difference decreases; that is, the smaller the seam length is, the faster the pressure difference rises and the faster the plugging speed. The mud-cake layer refers to the outer mud cake formed in the punching unit. The particle-size comparison of the mud-cake layer of the punching unit with different seam lengths is shown in Fig. 15(b). The particle-size distribution of the mud-cake layer of punching units with different seam lengths is similar, and the average heterogeneity coefficient of punching units with different seam lengths is $UC_L = 1.2410$.

As shown in Fig. 16(a), the amount of sand produced by a single punching unit increases with increasing seam length. This is because the volume of the punching unit increases with increasing seam length, the sand particles that can be accommodated increase, and the concentration of particles smaller than the opening height is much higher than that of particles larger than the opening height, resulting in an increase in the sand produced. Combined with the production site data, for the same size of plate, the seam is arranged in parallel, the spacing between the circular seam and the seam is 3.3 mm, and the spacing between the axial seam and the seam is 5 mm. The opening rates, 8, 11, 15 and 18 mm, are 4.5%, 4.8%, 5.7% and 6.2%, respectively. Due to different size parameters, the number of punching slots that can be accommodated on the same plate is different. In the following section, the total sand production refers to the product of the sand production of a single punching slot and the number of punching slots for the same plate. As shown in Fig. 16(b), both the total sand production and the porosity increase with increasing fracture length. The sand production of the punching unit with a fracture length of 15 mm is moderate, and the increase in the porosity is greater than that of the sand production. The opening rate is 26.7% higher than that of the punching unit with a seam length of 8 mm, and the final penetration rate ratio is the highest. From a comprehensive analysis, the recommended seam length of the punching screen is 15 mm in design.

4.1.2. *Punching screen unit seam width dimensions*

Only considering the influence of the seam width factor on the sand control performance of the slot unit, the control variable method is adopted when the seam length is 11 mm, the opening height is 0.3 mm, and the seam width sizes are 3, 3.5, 4, and 4.5 mm to carry out the study. In this case, the change in the pressure difference and penetration rate ratio is shown in Fig. 17(a). There is no significant difference in the trend of penetration rate ratio with different seam widths and the results after plugging stabilization, which indicates that the seam width of the thrust punching screen unit has little influence on penetration rate ratio. The rate of differential pressure is slow at the initial stage of blockage, and the rate is fastest in the stage of blockage aggravation and becomes slow again in the stage of blockage stability. The increasing rate of

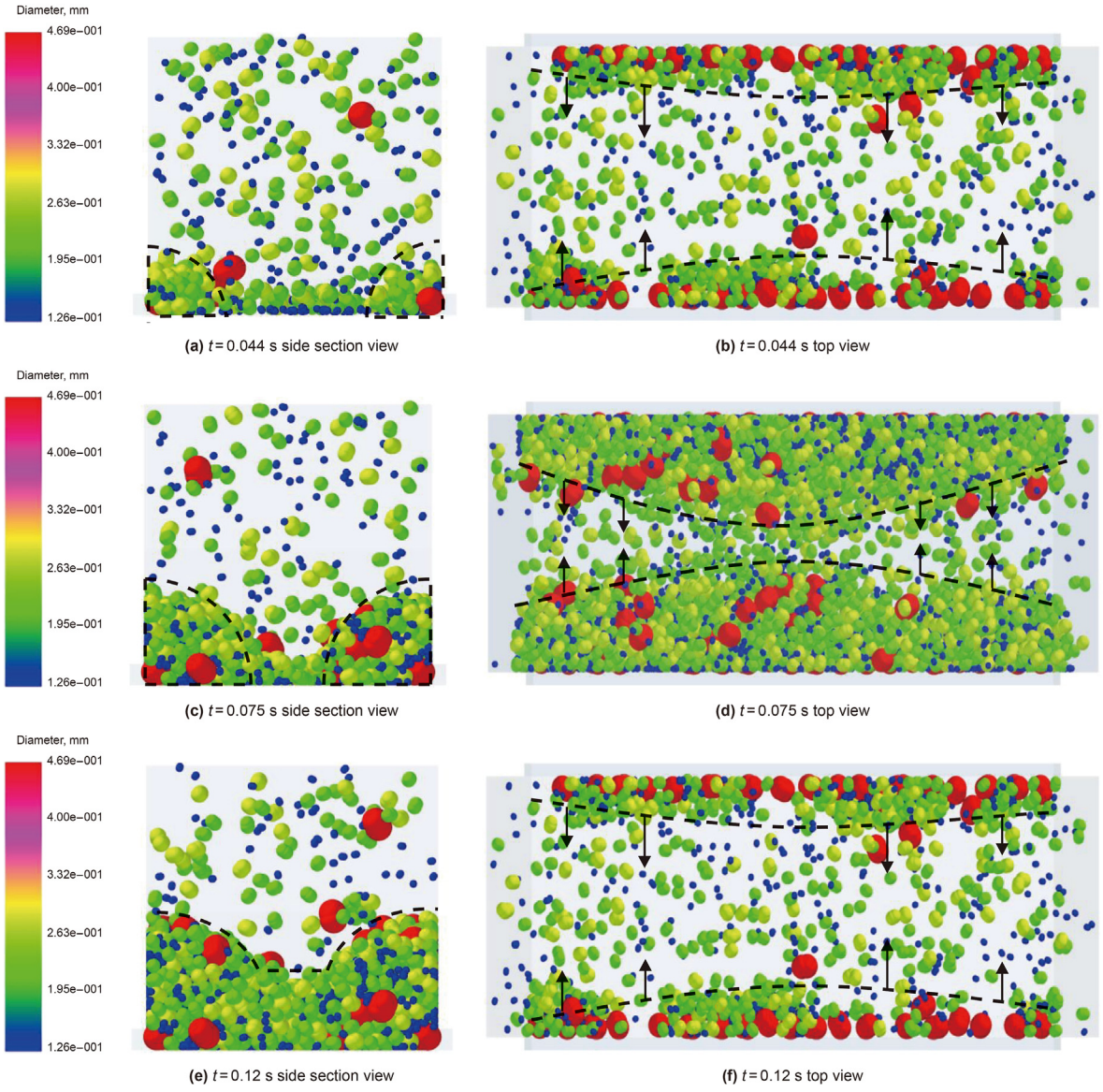

Fig. 12. Particle blockage state of nodes at different times.

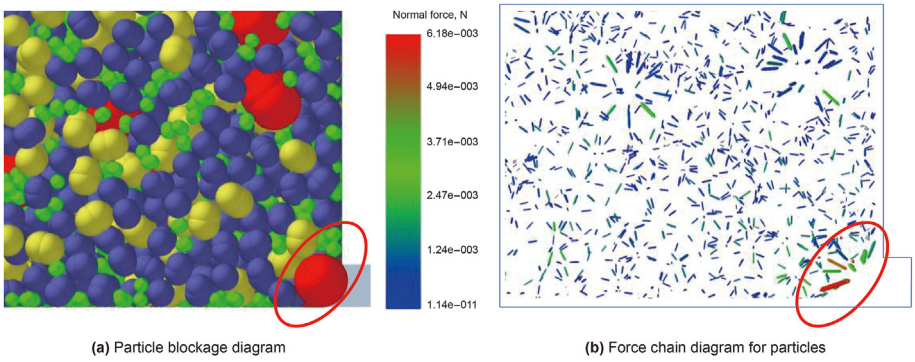

Fig. 13. Blocking form at the opening of the dead punching screen.

the pressure difference is lowest for a slit width of 3 mm, and the pressure difference is the smallest when plugging stability is reached; that is, the plugging rate and degree of plugging are the lowest for a slit width of 3 mm. When the slit width is 3.5 mm, the increasing trend of the pressure difference and the pressure difference after equilibration are similar to those when the slit width

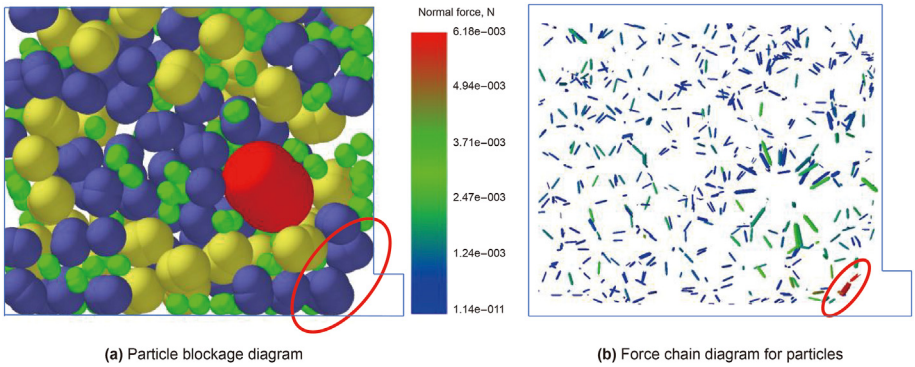

Fig. 14. Bridging patterns of particles at the slots of punching slot elements.

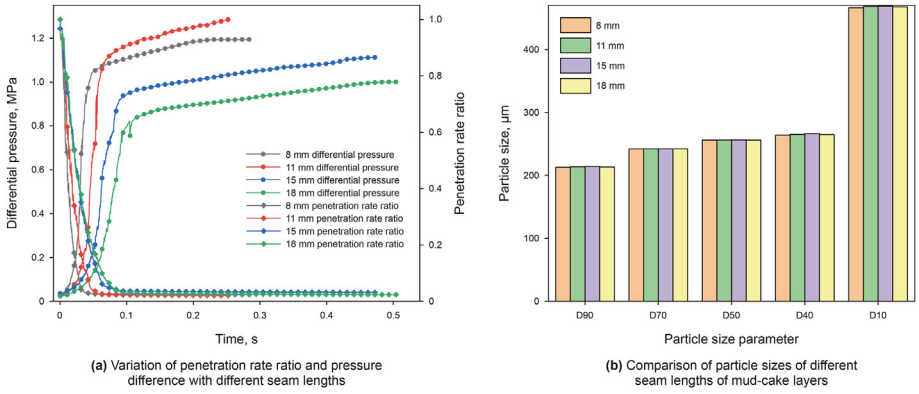

Fig. 15. Comparison of the pressure difference, penetration rate ratio and particle-size distribution of the mud-cake layer with different seam lengths.

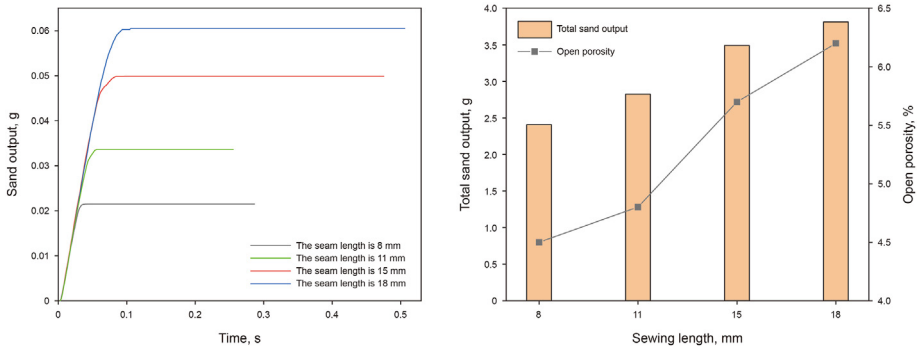

Fig. 16. Sand production and porosity of different slots.

is 3 mm. A seam width of 4 mm is similar to that of 4.5 and 5 mm, indicating that the clogging rate is approximately the same. The particle-size parameters of the mud-cake layer of the punching unit with different seam widths are very close to those in Fig. 17(b), and the average heterogeneity coefficient $UC_D = 1.2408$.

As shown in Fig. 18(a), with increasing seam width, the amount of sand produced generally shows a decreasing trend. This is because in the process of the seam width increasing from 3 to 5 mm, the amount of sand entering increases at the same time, but the opening size remains the same. There are more large particles, and the bridge structure more easily forms between the sand particles; therefore, the amount of sand produced decreases. There is little difference in the time needed to reach plugging stability for different seam widths. For the design of the punching screen, when the seam length is 11 mm, the opening height is 0.3 mm, the seam width is 3, 3.5, 4, and 4.5 mm, and the opening rates are 5.5%, 5.1%, 4.8%, 4.4%, and 4.1%, respectively. As shown in Fig. 18(b), both the total sand production and the opening rate decrease with increasing seam width. The sand production of the punching unit with a seam width of 3.5 mm is moderate, but the opening rate increases by 24.4% compared with that of the 5 mm seam width. The final penetration rate ratio of the punching unit with a seam width of 3.5 mm is the highest. Therefore, in a comprehensive analysis, it is recommended that the seam width of the punching screen is 3.5 mm when it is manufactured.

4.1.3. Opening height of the punching screen unit

Only the influence of the opening height on the sand control

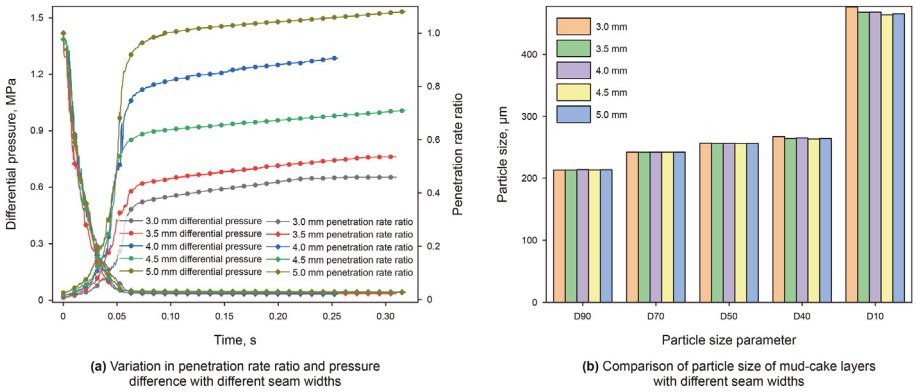

(a) Variation in penetration rate ratio and pressure difference with different seam widths

(b) Comparison of particle size of mud-cake layers with different seam widths

Fig. 17. Comparison of the pressure difference, penetration rate ratio and particle-size distribution of mud-cake layers with different seam widths.

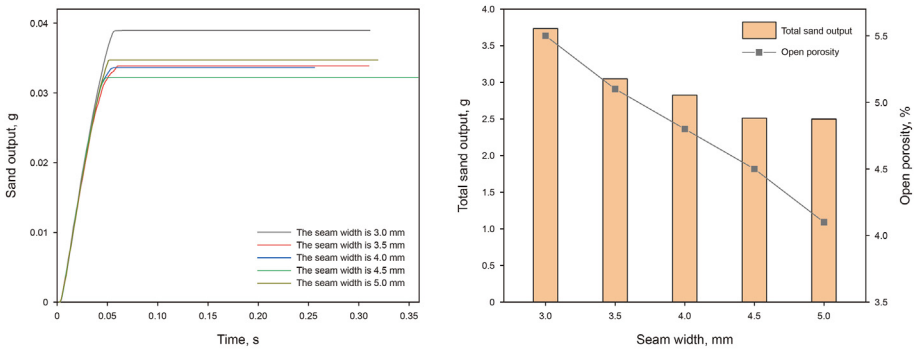

(a) Sand production of a single punching unit

(b) Total sand production and hole opening rate

Fig. 18. Sand production and hole opening rate with different seam widths.

performance of the slot unit is considered. When the seam length is 11 mm and the seam width is 4 mm, the control variable method is adopted to carry out the study by taking the opening height as 0.2, 0.25, 0.3, 0.35 and 0.4 mm. The penetration rate ratio changes are shown in Fig. 19(a), and the penetration rate ratio changes rapidly at the initial plugging. With the increase in the opening height, the penetration rate ratio rate decreases. The pressure difference varies greatly with the height of the opening. As the height of the opening increases, the growth rate of the pressure difference decreases, and the pressure difference decreases after reaching the stability of the plugging; that is, the larger the opening is, the lower the plugging rate and the lower the degree of plugging. Different opening heights of the mud-cake layer in regard to the particle size contrast, as shown in Fig. 19(b). Due to congestion and stability after the punched slot inside the unit formed a stable and dense sand layer, the mud-cake layer with tiny particles has difficulty breaking through the sand; therefore, different seam opening heights of the blunt unit mud-cake layer size distribution are similar, and the average coefficient of inhomogeneity is $UC_K = 1.2409$.

As shown in Fig. 20(a), sand production increases with increasing opening height. The difference in sand production between different opening heights is obvious. With an opening height of 0.4 mm the sand output is twice as high as with a 0.3 mm opening. When the opening height is 0.4 mm, the amount of sand produced is 8.4 times that of the 0.25 mm opening and 81 times that of the 0.2 mm opening. When the opening height is 0.2, 0.25,

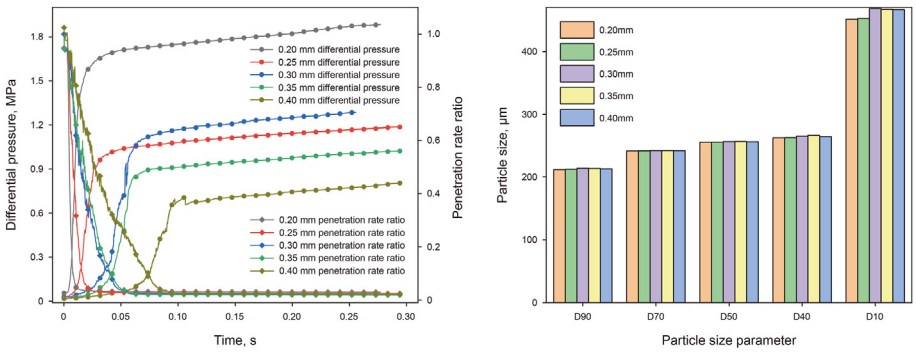

(a) Changes in penetration rate ratio and pressure difference at different opening heights

(b) Comparison map of particle size of mud-cake layer at different opening heights

Fig. 19. Comparison of pressure difference, penetration rate ratio and particle-size distribution of the mud-cake layer at different opening heights.

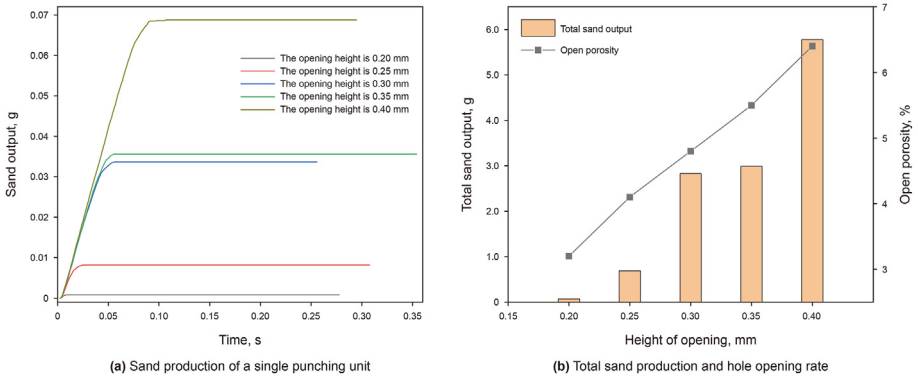

(a) Sand production of a single punching unit (b) Total sand production and hole opening rate

Fig. 20. Sand production and hole opening rate with different opening heights.

0.3, 0.35 and 0.4 mm, the time required to reach blockage stability is 0.011, 0.028, 0.058, 0.056 and 0.108 s, respectively. The figure shows that the plugging stability of the punching unit is more stable than that of the slotted screen sand, and there is no plugging failure after plugging stability. The opening rate of punching screen with different opening heights is shown in Fig. 20(b). With increasing opening height, the opening rate increases, and the opening height should be selected according to the corresponding principles of engineering practice.

5. Conclusion and discussion

(1) The clogging process of the punching screen generally shows three stages: beginning to clog, worsening of clogging, and stable clogging. There are two sand retaining forms in the punching screen: large particles stuck in the dead seam and sand bridge retaining sand.

(2) At the beginning of the blocking stage, larger particles preferentially aggregate at the streamline convergence point under the chamfering of the punching screen, forming a sparse bridge structure; at the stage of increasing the blockage, particle clusters are formed at the priority aggregation point of large particles, and then the particle clusters develop into a relatively complete sand bridge structure, showing that both ends of the opening develop to the center of the opening. In the stable plugging stage, the opening is “fan-shaped” stacking, forming a “V-shaped” valley inside the punching screen, which develops from the opening on both sides of the punching screen to the center.

(3) The larger the slot length of the punching screen is, the slower the plugging and the larger the sand production. With increasing slot length, the rate of permeability reduction decreases. The smaller the slot length is, the faster the pressure difference rises and the faster the plugging speed. Although the punching fracture unit is related to the actual field demand design, under a certain reservoir particle-size condition, the sand production increases sharply with the increase in the opening height; the slower the permeability ratio decreases, the smaller the plugging rate and the lower the plugging degree. The penetration rate, plugging rate and plugging degree are not significantly affected by the width of the punching unit.

(4) In the actual production process, the controllable factors affecting the clogging of the punching screen are the seam length and the height of the opening. Considering the influence of structural dimension parameters on permeability, sand production and opening rate, it is recommended that the seam length and width of the punching screen should be 15 and 3.5 mm, respectively.

(5) Through the plugging mechanism analysis of the punching unit with different seam lengths, seam widths and opening heights, it is found that when equilibrium is reached, the difference between the final permeability of different seam lengths, seam widths and opening heights is less than 0.01. The grain-size distribution of the punching element with different sizes among the factors is similar. The average heterogeneity coefficients of the punching element with different seam lengths, seam widths and opening heights are $UC_L = 1.2408$, $UC_D = 1.2407$ and $UC_K = 1.2409$, respectively. Based on the above analysis, it is believed that the final permeability of the punching element may be independent of the size parameters. It is only related to the permeability of the mud-cake layer after the plugging and stabilization of the sluicing unit.

Declaration of competing interest

The authors declare that they have no known competing financial interests or personal relationships that could have appeared to influence the work reported in this paper.

References

Cheng, K., Wang, Y., Yang, Q., 2018. A semi-resolved Cfd-dem model for seepage-induced fine particle migration in gap-graded soils. Comput. Geotech. 100, 30–51. https://doi:10.1016/j.compgeo.2018.04.004.

Deng, F., Deng, Z., Liang, H., Wang, L., Hu, H., Xu, Y., 2021. Life prediction of slotted screen based on back-propagation neural network. Eng. Fail. Anal. 119, 1–8. https://doi.org/10.1016/j.engfailanal.2020.104909.

Deng, F., Feng, Y., Yan, C., Lin, H., Gong, N., Wang, J., 2017a. Experimental investigation of factors affecting gravel pack efficiency for thermal recovery wells in Bohai Bay, China. J. Petrol. Sci. Eng. 156, 835–844. https://doi.org/10.1016/j.petrol.2017.06.054.

Deng, F., Li, X., He, L., Feng, Y., 2019. Experimental evaluation of metal foam for sand control. J. Petrol. Sci. Eng. 176, 1152–1160. https://doi.org/10.1016/j.petrol.2019.01.087.

Deng, F., Lin, H., Cao, Y., Pan, H., Yan, W., 2017b. Experimental study of plugging mechanisms of metal mesh screens with different particle compositions. Petroleum Science Bulletin 2 (4), 500–506. https://doi:10.3969/j.issn.2096-1693.2017.04.046 (in Chinese).

Deng, F., Shen, X., Liang, Q., Wang, L., Wang, J., Deng, Z., Wei, J., 2018. The jamming mechanism of sand control screen for the montmorillonite inflation with the water. J. Pet. Explor. Prod. Technol. 8 (1), 189–194. https://doi.org/10.1007/s13202-017-0329-z.

Deng, F., Yin, B., Li, X., Wang, Y., Xu, Y., 2022. Analysis of the scaling mechanism and characteristics of a double-defects screen based on data from Hafaya Oilfield. J. Petrol. Sci. Eng. 216, 1–12. https://doi.org/10.1016/j.petrol.2022.110729.

Dong, C., Gao, K., Zhou, C., Zhi, Q., Li, H., Zhang, Q., 2016. Experimental study of sand retaining media plugging pattern in sand control well and quantitative prediction model for plugging degree. J. Exp. Mech. 32 (3), 351–360. https://doi:10.7520/1001-4888-16-047 (in Chinese).

Feng, Y., Ma, C., Chu, M., Zhong, Y., Deng, J., 2021. Numerical simulation on the

mechanism for rigid particle plugging of leakage in fracture formations. Nat. Gas. Ind. 41 (7), 93–100. https://doi.org/10.3787/j.issn.1000-0976.2021.07.010 (in Chinese).
Gillespie, G., Deem, C.K., Malbrel, C., 2000. Screen selection for sand control based on laboratory tests. In: SPE Asia Pacific Oil and Gas Conference and Exhibition. https://doi.org/10.2118/64398-MS.
Ismail, N.I., Kuang, S., Yu, A., 2020. CFD-DEM study of particle-fluid flow and retention performance of sand screen. Powder Technol. 378 (PA), 410–420. https://doi.org/10.1016/j.powtec.2020.10.012.
Kuang, S., Zhou, M., Yu, A., 2020. CFD-DEM modelling and simulation of pneumatic conveying: a review (prepublish). Powder Technol. 365, 186–207. https://doi.org/10.1016/j.powtec.2019.02.011.
Li, M., 2019. Optimization of Structural Parameters of Screen Punching Type Protective Shell. China University of Petroleum, Beijing. https://10.27643/d.cnki.gsybu.2019.000346 (in Chinese).
Li, Q., Wu, J., 2022. Factors affecting the lower limit of the safe mud weight window for drilling operation in hydrate-bearing sediments in the northern south China sea. Geomech. Geophys. Geo-energy Geo-resour. 8 (2), 82. https://doi.org/10.1007/s40948-022-00396-0.
Li, Q., Han, Y., Liu, X., Ansari, U., Cheng, Y., Yan, C., 2022. Hydrate as a by-product in Co2 leakage during the long-term sub-seabed sequestration and its role in preventing further leakage. Environ. Sci. Pollut. Control Ser. 29 (51), 77737–77754. https://doi.org/10.1007/s11356-022-21233-7.
Li, W., Qian, J., Yin, Z., Zhou, C., 2021. Simulation of seepage erosion in gap graded sand soil using CFD-DEM. Rock Soil Mech. 42 (11), 3191–3201. https://doi.org/10.16285/j.rsm.2021.0123 (in Chinese).
Li, W., Wang, J.a., Duan, X., Zu, H., Liu, H., Yao, H., Shi, B., Gong, J., 2020. Hydrate blockage simulation based on CFD-DEM coupling method. Oil Gas Storage Transp. 39 (12), 1379–1385. https://10.6047/j.issn.1000-8241.2020.12.010 (in Chinese).
Lu, J., Wu, S., Li, D., Liang, D., Wei, W., He, Y., Shi, L., Deng, F., Xiong, Y., 2022. Solid phase control strategy during the exploitation of marine gas hydrates. Adv. New Renew. Energy 10 (2), 137–145. https://doi:10.3969/j.issn.2095-560X.2022.02.006.
Qing, Y., Kuang, C., Yin, W., Mahmood, A., 2019. Improvement of semi-resolved Cfd-dem model for seepage-induced fine-particle migration: eliminate limitation on mesh refinement. Comput. Geotech. 110, 1–18. https://doi.org/10.1016/j.compgeo.2019.02.002.
Song, Y., Ranjith, P., Wu, B., Song, Z., 2021. A microscopic study of sand arches and sand skeletons under hydrodynamic force based on the CFD-DEM model. J. Nat. Gas Sci. Eng. 92, 1875–5100. https://doi.org/10.1016/j.jngse.2021.104017.
Wang, Y., Cheng, K., Yang, Y., Tao, Y., Li, Y., 2022. Microscopic mechanical analysis of sand production using a new arbitrary resolved-unresolved Cfd-dem model. Int. J. Multiphase Flow 149, 103979. https://doi.org/10.1016/j.ijmultiphaseflow.2022.103979.
Xu, B., Yu, A., 1997. Numerical simulation of the gas-solid flow in a fluidized bed by combining discrete particle method with computational fluid dynamics. Chem. Eng. Sci. 52 (16), 2785–2809. https://doi.org/10.1016/S0009-2509(97)00081-X.
Yang, S, 2018. Experimental Study on Blocking Mechanism of Sand Control Screen in Sand-Shale Interbed. China University of Petroleum (East China). https://doi.org/10.1080/02726351.2018.1547341.
Yao, Y., Guo, Z., Zeng, J., Li, D., Lu, J., Liang, D., Jiang, M., 2021. Discrete element analysis of hydraulic fracturing of methane hydrate-bearing sediments. Energy Fuels 35 (8), 6644–6657. https://doi.org/10.1021/acs.energyfuels.1c00248.
Yin, B., Deng, F., Shen, X., Chen, S., Wen, M., 2021. Research on simulation of scaling rate in slotted screen pipe. J. Saf. Sci. Technol. 17 (9), 120–125. https://doi:10.11731/jissn1673-193x (in Chinese).
Zhang, Z., 2017. An Advanced sand Control Technology for Heavy Oil. Reservoirs Graduate Studies.
Zhang, Y., Wang, W., Zhang, P., Li, G., Tian, S., Lu, J., Zhang, B., 2022. A solution to sand production from natural gas hydrate deposits with radial wells: combined gravel packing and sand screen. J. Mar. Sci. Eng. 10 (1), 71. https://doi.org/10.3390/jmse10010071. https://www.mdpi.com/2077-1312/10/1/71.